AAS 24-012

NEW PERSPECTIVE ON SLOSH DYNAMICS IN HIGH-GRAVITY REGIMES FOR LUNAR MISSIONS

Han Woong (Brian) Bae [*] **Kevin Geohagan**[†] **Kelly Barber** [‡] **Ravi Purandare** [§] **and Juan Orphee** [¶]

Slosh dynamics particularly in high gravity regime is of high interest to the NASA Human Landing Systems program, which aims to return humans to the Moon. This paper reexamines the commonly accepted equivalence between pendulum and mass-spring-damper mechanical analogies, demonstrating the differences through simulations and their impact on design and analysis. This study re-derives equations of motion for these mechanical models including mass-spring-damper (MSD) and pendulum by relaxing simplifying assumptions that had been typically applied to large launch vehicles and may be violated for lunar and planetary landing applications. The newly-derived equations uncover potential modeling gaps when applying the pendulum and MSD models, and the need for additional considerations in their application. Finally, the newly-derived equations are validated using MathWorks® Simscape™ Multibody™ dynamics toolbox simulation.

INTRODUCTION

The dynamic behavior of liquid sloshing within tanks has been recognized as a critical consideration in the design of the space vehicles, particularly in the context of guidance, navigation and control (GNC). The high-gravity slosh model has been extensively used in the past, where the mechanical analogies such as the pendulum and MSD models have been employed to approximate slosh dynamics. This approach has worked well for launch vehicles, which involve slow dynamics.

The NASA Human Landing System (HLS) program, tasked with returning humans to the Moon and Mars, demands a deeper understanding of slosh dynamic in environments fundamentally different from Earth-based launch vehicle applications. Lunar landing missions involve smaller tanks and highly dynamic motion profiles, all of which may violate the simplifying assumptions typically used in slosh modeling in larger Earth-based launch vehicles. For example, the multi-body dynamics derivation for Space Launch System (SLS) in Space Transportation and Aeronautics Research Simulation (STARS) six degree of freedom simulation has some assumptions that take out nonlinear and secondary terms of the slosh dynamics out of the vehicle rotational equation of motion. This type of simplification may not provide an accurate solution for lunar landers [1].

[*]Aerospace Engineer, Control Systems Design and Analysis Branch, NASA Marshall Space Flight Center, Huntsville, AL 35808.

[†]Aerospace Engineer, Control Systems Design and Analysis Branch/ESSCA, NASA Marshall Space Flight Center, Huntsville, AL 35808.

[‡]Aerospace Engineer, Control Systems Design and Analysis Branch/ESSCA, NASA Marshall Space Flight Center, Huntsville, AL 35808.

[§]Aerospace Engineer, Vehicle Struture and Dynamics Branch, NASA Marshall Space Flight Center, Huntsville, AL 35808.

[¶]Aerospace Engineer, Control Systems Design and Analysis Branch, NASA Marshall Space Flight Center, Huntsville, AL 35808.

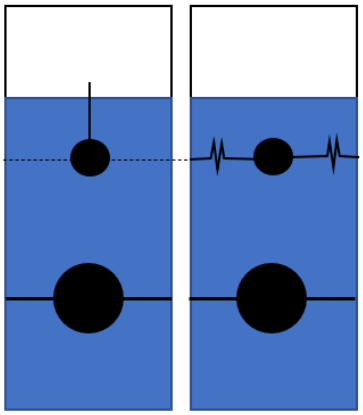

(a) Pendulum mass and mass-spring mass located on the same height

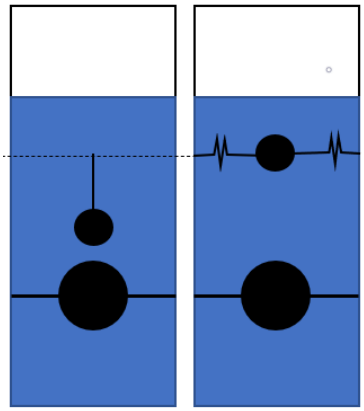

(b) Pendulum hinge point and mass-spring mass located on the same height

Figure 1: Two different cases of pendulum and mass-spring equivalency analogies

Furthermore, there are common confusions regarding the equivalence of mass spring damper and pendulum analogies. In Refs. [2] and [3], the authors suggest locating the MSD mass at the same elevation as the pendulum mass and not at the pendulum hinge point location as depicted in Figure 1a. On the other hand, Refs. [4] assume the pendulum hinge point is aligned with the MSD mass as depicted in the analogy in Figure 1b. Similarly, another well-known slosh parameter determination guideline (SP-106) in ref. [5] shows misaligned MSD and pendulum mass locations in the lower half of the fill level such that it does not follow the cases shown in 1a or 1b. Both pendulum and MSD mechanical analogies are commonly used in control design and analysis for space vehicles; however, pendulum models are often avoided due to a lack of clarity regarding the equivalence of their dynamics. To address this uncertainty and build confidence in pendulum models, an in-depth study was conducted to examine the effects of pendulum hinge point locations in comparison with the MSD model, aiming to identify and quantify the discrepancies that arise when these models are applied.

In addition, the paper will go into details on the treatment of the equation of motion (EOM) for the effect of the sloshing torque on the vehicle due to the sloshing lateral offset and the proper acceleration, the so-called k_3 or $\bar{g}_0$, first introduced by Frosch et al. [6] and adopted in later literature [1, 4, 7, 8]. This effect is a critical element of the vehicle dynamic that has been carefully implemented in previous studies. The paper will discuss how each mechanical model captures the effect of vehicle rotational dynamics due to the slosh lateral offset and clarify common misconceptions and errors associated with the application of the k_3 term.

The paper specifically derives multibody dynamics equations of motion for both pendulum and MSD models, maintaining most of the nonlinear and secondary terms that were typically omitted in the Earth-based launch vehicle problems. These equations of motion are then verified and validated with MathWorks® Simscape™ Multibody™, bringing higher confidence in both derived mathematics and slosh-vehicle multibody dynamics modeled using Simscape™ Multibody™.

Furthermore, The EOMs for MSD and pendulum models along with corresponding Simscape™ models, have been integrated into GeneraLized Aerospace Simulation in Simulink® (GLASS), which is a six-DOF flight simulation tool used at NASA Marshall Space Flight Center to evaluate

lunar lander vehicles. Its core engine is built on Matlab® Simulink® and MathWorks® Simscape™ Multibody™ dynamics toolbox.

Summarizing, the paper derives the EOMs for pendulum and MSD models, validates the slosh modeling in GLASS via Simscape™ Multibody™, identifies and discusses the common errors and misconceptions associated with the applications of these models, and provides recommendations for their proper use in simulations and analyses.

Figures 2a and 2b show a simplified diagram of the space vehicle with a single TVC and jth slosh mass in both MSD and pendulum representations. For simplicity, the EOM derivation assumes negligible nozzle dynamics.

The slosh parameters are obtained using the Marshall Space Flight Center's WINSLOSH tool that is built based on NASA's SP-8009 [3]. This tool also follows the guideline from Dodge's book [2] on the location of the pendulum mass at the same location as the MSD mass location.

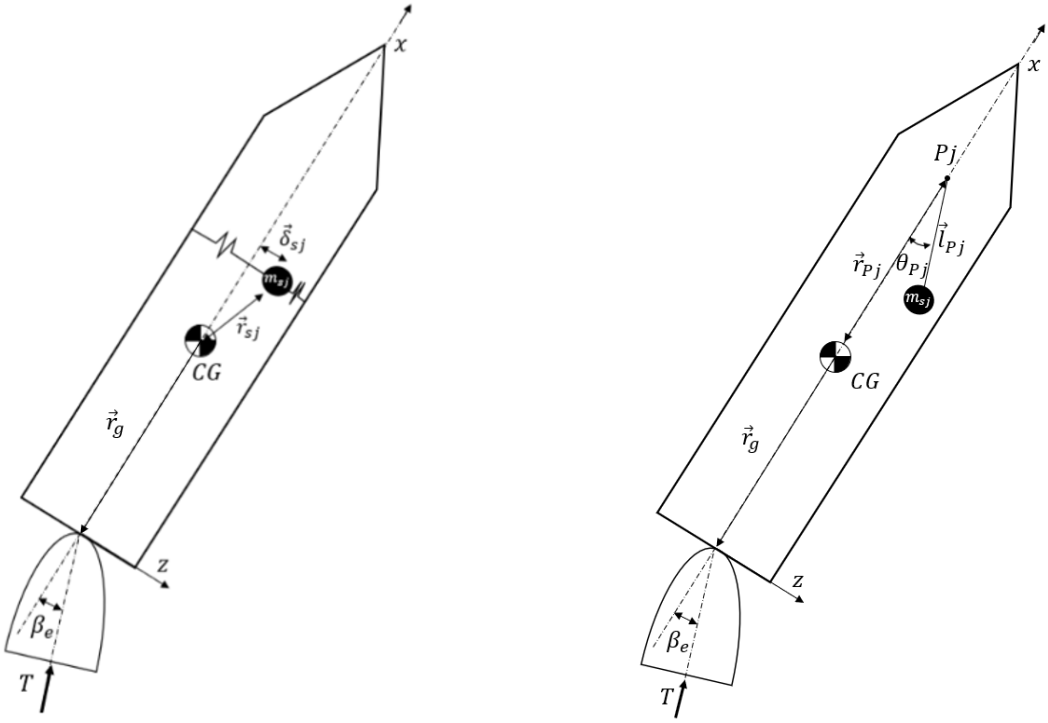

(a) Simple Single TVC and MSD jth Slosh Space Vehicle Dynamic

(b) Simple Single TVC and Pendulum jth Slosh Space Vehicle Dynamic

Figure 2: Diagram of Simple Single TVC Space Vehicle with jth Slosh Mass for MSD and Pendulum Analogies

Mass Spring Damper EOM Derivation

The rate of linear momentum differentiated with respect to the body axis is given by:

$$\dot{\vec{p}} = -\vec{\omega} \times \vec{p} + \vec{f} \tag{1}$$

The rate of change of rotational momentum differentiated with respect to the body axis is given by:

$$\dot{\vec{h}} = -\vec{\omega} \times \vec{h} + \vec{g} \tag{2}$$

Deriving the momentum and utilizing Equations 1 and 2 (Appendix A), the derivation yields the moving slosh mass EOM:

$$\ddot{\vec{\delta}}_{sj} + D\dot{\vec{\delta}}_{sj} + K\vec{\delta}_{sj} = -\vec{a}_b + \vec{r}_{sj} \times \dot{\vec{\omega}} + \vec{\omega} \times (\vec{\omega} \times \vec{r}_{sj}) - 2\vec{\omega} \times \dot{\vec{\delta}}_{sj} \tag{3}$$

where $D = 2\zeta_{sj}\omega_{sj}$ and $K = \omega_{sj}^2$. The vehicle body's translational EOM is:

$$m_T\vec{a}_b = \vec{T}_e + m_{sj}(K\vec{\delta}_{sj} + D\dot{\vec{\delta}}_{sj}) \tag{4}$$

Vehicle body's rotational EOM is:

$$\begin{aligned} I_T\dot{\vec{\omega}} = -\vec{\omega} \times I_T\vec{\omega} - m_{sj}\vec{r}_{sj} \times \vec{a}_b - m_{sj}\vec{r}_{sj} \times \ddot{\vec{\delta}}_{sj} + m_{sj}\vec{r}_{sj} \times (\vec{r}_{sj} \times \dot{\vec{\omega}}) \\ + m_{sj}\vec{r}_{sj} \times (\vec{\omega} \times (\vec{\omega} \times \vec{r}_{sj})) - 2m_{sj}\vec{r}_{sj} \times (\vec{\omega} \times \dot{\vec{\delta}}) + \vec{r}_g \times \vec{T}_e \end{aligned} \tag{5}$$

Pendulum EOM Derivation

Using Newton-Euler method:

$$\Sigma\vec{F} = m\vec{a} \tag{6}$$

$$\Sigma\vec{M} = \frac{\partial\vec{h}}{\partial t} + \vec{\omega} \times \vec{h} \tag{7}$$

Derivation (Appendix B) yields the pendulum slosh mass EOM:

$$\ddot{\vec{\theta}}_{Pj} = \frac{\vec{l}_{Pj} \times \left(\frac{\vec{T}}{m_T} - \dot{\vec{\omega}} \times \vec{r}_{Pj} - \vec{\omega} \times (\vec{\omega} \times \vec{r}_{Pj})\right)}{|\vec{l}_{Pj}|^2} - \dot{\vec{\omega}} \tag{8}$$

And the force imparted on the vehicle at the pivot point:

$$\begin{aligned} \vec{f} = m_{sj}\Big\{ -\ddot{\vec{\theta}}_{Pj} \times \vec{l}_{Pj} - \dot{\vec{\theta}}_{Pj} \times \dot{\vec{\theta}}_{Pj} \times \vec{l}_{Pj} - 2\vec{\omega} \times \left(\dot{\vec{\theta}} \times \vec{l}_{Pj}\right) \\ -\vec{a}_b - \dot{\vec{\omega}} \times \left(\vec{r}_{Pj} + \vec{l}_{Pj}\right) - \vec{\omega} \times \left[\vec{\omega} \times \left(\vec{r}_{Pj} + \vec{l}_{Pj}\right)\right] \Big\} \end{aligned} \tag{9}$$

Vehicle body's rotational EOM is:

$$I_T\dot{\vec{\omega}} = -\vec{\omega} \times I_T\vec{\omega} + m_{sj}\vec{r}_{Pj} \times \left\{ -\ddot{\vec{\theta}}_{Pj} \times \vec{l}_{Pj} - \dot{\vec{\theta}}_{Pj} \times \dot{\vec{\theta}}_{Pj} \times \vec{l}_{Pj} - 2\vec{\omega} \times \left(\dot{\vec{\theta}} \times \vec{l}_{Pj} \right) \right.$$
$$\left. -\vec{a}_b - \dot{\vec{\omega}} \times \left(\vec{r}_{Pj} + \vec{l}_{Pj} \right) - \vec{\omega} \times \left[\vec{\omega} \times \left(\vec{r}_{Pj} + \vec{l}_{Pj} \right) \right] \right\} + \vec{r}_g \times \vec{T}_e \tag{10}$$

EOM VALIDATION

Validation Set-up

To verify the equations of motion developed above, a test environment was constructed using the MathWorks® Simscape™ Multibody™ toolbox. The testing environment consists of a "cart" body which is free to translate along the X and Y axes, to which a "tank" body is affixed via a hinge which is free to rotate about the Z axis. This mechanism as shown in Figure 3 is used to examine the coupled vehicle-slosh dynamic behavior of the MSD and pendulum slosh mathematical models detailed in the subsections above.

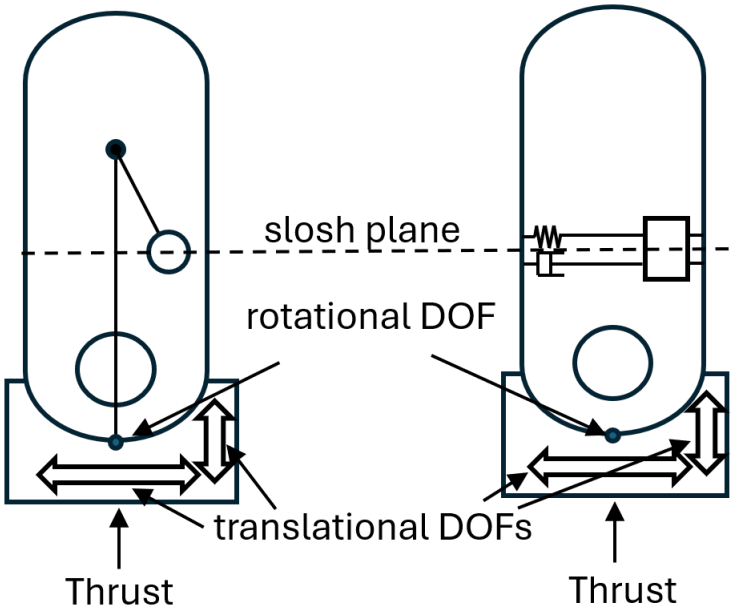

Figure 3: Illustration of Comparison Test Setup

The mass-spring-damper and pendulum slosh models derived in the subsections above were implemented in MathWorks® Simulink® and Matlab® along with "truth" mass-spring-damper and pendulum slosh mechanism models built using the Simscape™ Multibody™ toolbox.

In order to validate the derivation of the models, comparisons were conducted between the Simscape™ Multibody™ "truth" models and the corresponding Matlab® and Simulink® model. These comparisons consist of 3 parts:

- Comparison of the motion of the slosh mass within the moving tank frame. The equations of motion for both math models yield the dynamics in the local tank frame.
- Comparison of the tilting motion of the tank in response to slosh motion. Because slosh motion is not only influenced by vehicle motion but also influences vehicle motion, an examination of the motion of the coupled body is required for complete validation of each model.
- Comparison of the translational motion of the tank in response to slosh motion. Similar to the tank tilting comparison, this is to ensure that the translational degrees of freedom exhibit the same motion.

See the flow diagram in Figure 4 detailing the modeling and comparison process.

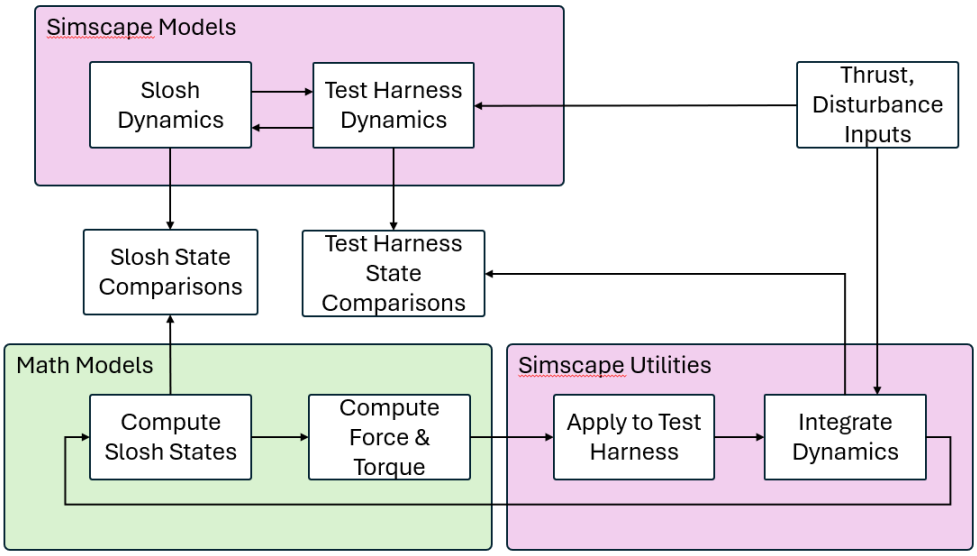

Figure 4: Illustration of Simulation, Comparison Process

Validation Results

Comparisons of the derived equations with the corresponding Simscape™ Multibody™ "truth" model showed matching dynamics for the slosh mass (shown in Figure 5), tank/vehicle tilt, and tank/vehicle translation with no damping active.

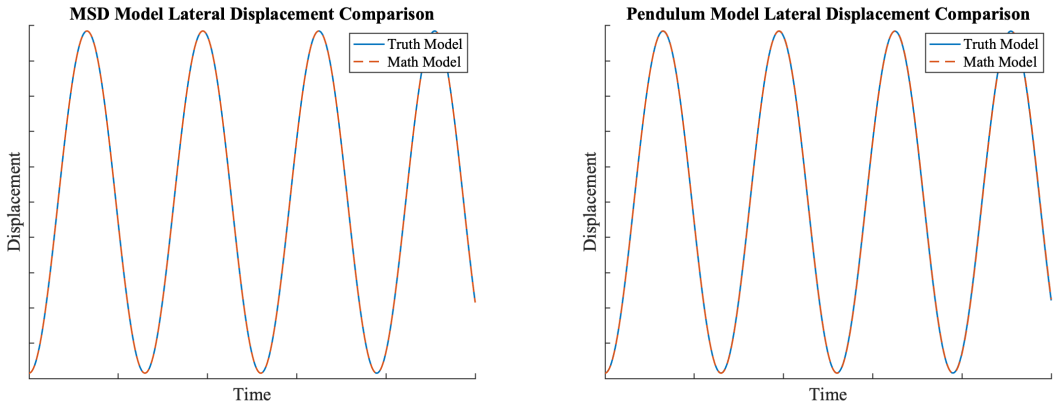

(a) MSD model (b) Pendulum model

Figure 5: EOM Model comparison to Simscape™ (Truth Model) with no damping

The math model performance when damping is active (shown in Figure 6) indicates a problem with the implementation of damping for the pendulum model. Work to identify the damping issue is ongoing.

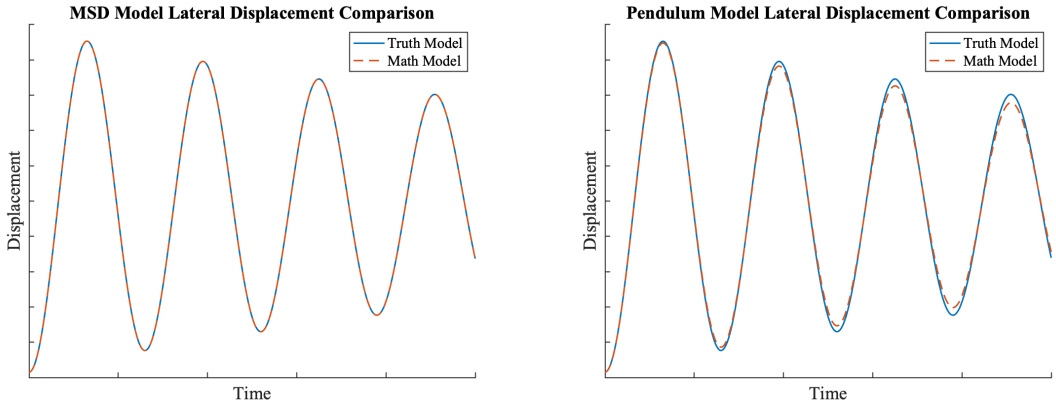

(a) MSD model (b) Pendulum model

Figure 6: EOM Model comparison to Simscape™ (Truth Model) with slosh damping active

As shown in Figures 5 and 6, validation testing consisted of single-plane motion only; for a comparison between MSD and pendulum models without the single-plane limitation, see the section titled ”GLASS Simulation Results”.

ANALYSIS AND INTERPRETATION

In this section, the implications of the k_3 effect in the newly-derived EOM will be discussed. Furthermore, the comparison between cases a) from Figure 1a (pendulum sloshing mass location located on MSD sloshing mass location) and b) from Figure 1b (pendulum hinge point located on MSD sloshing mass location) will be discussed.

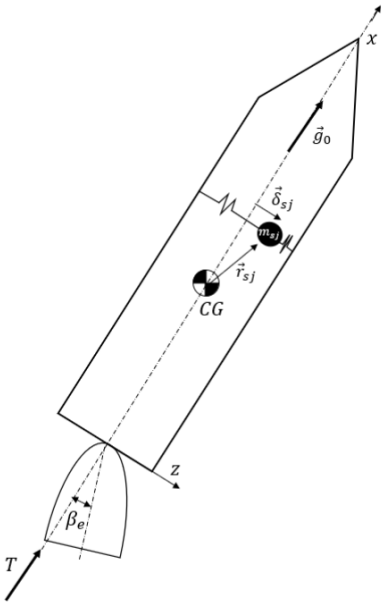

(a) k_3 or $\bar{g}_0$ configuration used in other literature

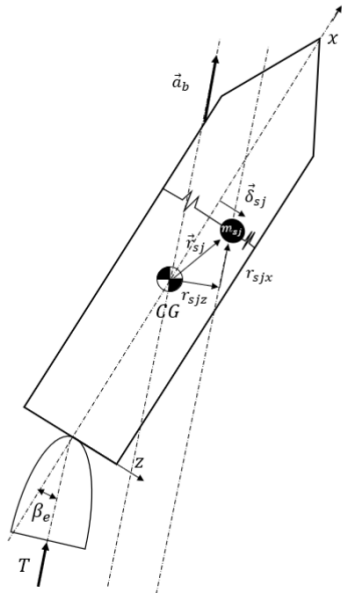

(b) The moment arm effect of $\vec{r}_{sjz}$ due to $\vec{a}_b$.

Figure 7: Comparison between common k_3 or $\bar{g}_0$ assumptions and Proposed EOM.

Implications to the Proper Axial Acceleration

The vehicle rotational EOM derived with the MSD model in the previous section is shown in the following:

$$I_T\dot{\vec{\omega}} = -\vec{\omega} \times I_T\vec{\omega} - m_{sj}\vec{r}_{sj} \times \vec{a}_b - m_{sj}\vec{r}_{sj} \times \ddot{\vec{\delta}}_{sj} + m_{sj}\vec{r}_{sj} \times (\vec{r}_{sj} \times \dot{\vec{\omega}}) + m_{sj}\vec{r}_{sj} \times (\vec{\omega} \times (\vec{\omega} \times \vec{r}_{sj})) - 2m_{sj}\vec{r}_{sj} \times (\vec{\omega} \times \dot{\vec{\delta}}) + \vec{r}_g \times \vec{T}_e \quad (11)$$

In this equation, there is no variable or term that directly indicates the proper axial acceleration and the lateral displacement of slosh, but this effect is already implicated in the equation and captures higher details and fidelity compared to the simplified approach.

In various simulation set-ups and analyses including [1, 4, 6, 7], the slosh torque effect on the vehicle due to slosh lateral offset and the proper acceleration, so called k_3 or $\bar{g}_0$, is depicted in Figure 7a. This approach commonly assumes that the main thrust of the vehicle is aligned with the axial axis of the vehicle. This effect is similarly captured in the new EOM where it captures moment due to the $\vec{a}_b$ vector—that is not always aligned with the body axial vector—and the moment arm r_{sjz} of the sloshing mass with respect to the $\vec{a}_b$ vector. This leads newly-derived EOM to capture not only the k_3 effect, but the effect of the lateral acceleration of the vehicle, mainly stemming from the deflected Thrust Vector Control (TVC) angle.

Furthermore, the newly-derived pendulum EOM does not show any variable or term explicitly related to k_3. The following subsection will discuss how pendulum model inherently accounts for the k_3 effect through an alternative perspective.

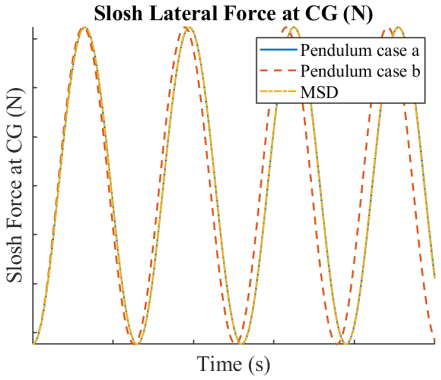

(a) Comparison of Pendulum slosh lateral force at CG for cases a) and b)

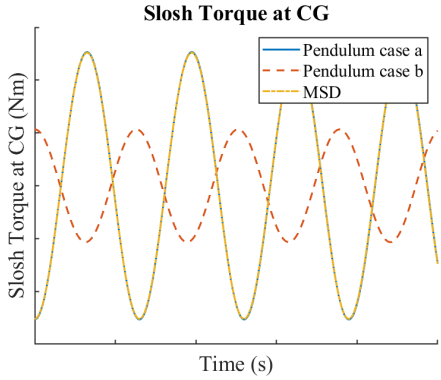

(b) Comparison of Pendulum slosh torque at CG for cases a) and b)

Figure 8: Comparison of Pendulum slosh lateral force and torque at CG for cases a) and b)

Comparison Test Results and Findings

This test looks at two different settings associated with pendulum hinge point locations—case a) and b) as shown in Figures 1a and 1b. The results in Figures 8a and 8b show that case a)—where the pendulum mass is located at the same level as the MSD mass—leads to match in torque and force, while case b)—where the pendulum hinge point is located at the same level as the MSD mass—leads to mismatch.

It is noteworthy that while the lateral forces and torques are identical for the pendulum and MSD models shown in case a), the force application points differ by the pendulum length between two models as seen in Figure 9. When looking at axial moment arm and lateral forces only, one must expect that case a) pendulum model would yield higher torque. However, the pendulum model in case a) and the MSD models yield comparable torque. The reason for the equivalent torques is that the pendulum model inherently captures MSD's torque effect due to the lateral offset of the moving slosh mass. As seen in Figure 9 in the MSD model, the axial force f_x imparted by the slosh moving mass involves torque due to the lateral offset of the moving slosh mass, while the pendulum model shows the axial force f_x aligned with the center of gravity and does not torque due to the axial force.

In Figure 10, the torque effect due to slosh can be broken into torque effects from axial and lateral force effects. It is observed that the MSD torque from the axial force effect is comparable with the pendulum lateral force multiplied with the pendulum arm length whereas

$$\delta_{sjx} f_{sjx} \approx L_{Pj} f_{sjz} \tag{12}$$

where f_{sjx} is equivalent to the slosh mass times the proper axial acceleration, or so called k_3 or $\bar{g}_0$.

The above observation shows that the extra torque yielded by the longer axial moment arm in pendulum model makes up for the missing explicit lateral slosh mass offset effect. For this reason, recommendations by established guidelines from [2, 3] to position the pendulum mass at the same level as the MSD mass more accurately capture the integrated torque effect compared to cases where neither the pendulum hinge point nor the pendulum mass aligns with the MSD mass [5].

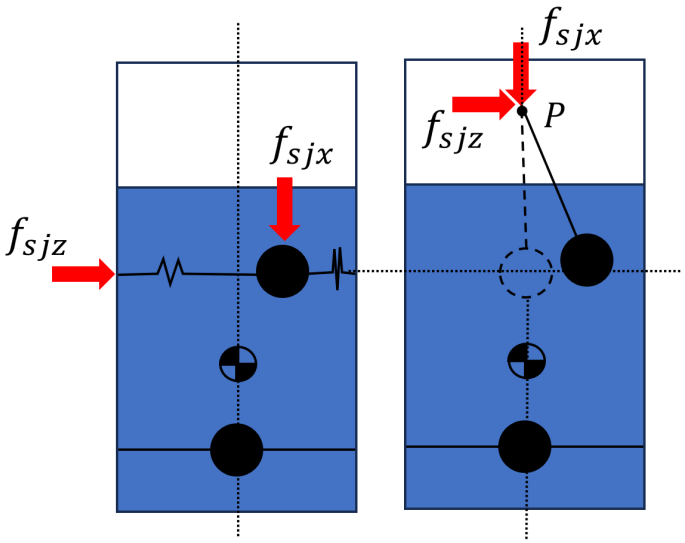

Figure 9: Diagram of the pendulum and MSD analogies including locations of the force components

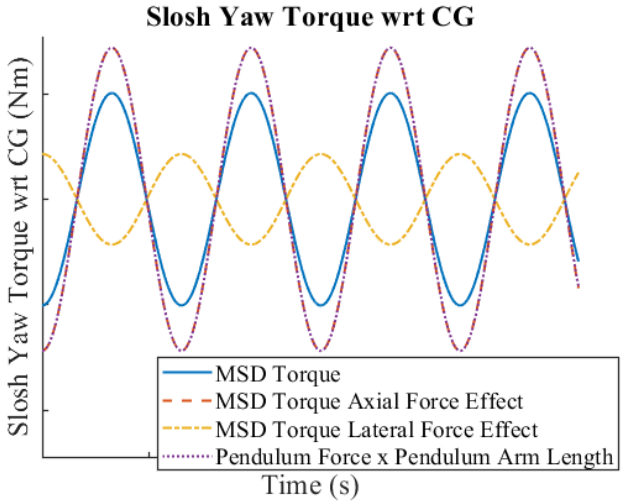

Figure 10: Slosh yaw torque at CG with MSD axial and lateral force effects

Implications of the Pendulum Model to the Danger Zone

A rule-of-thumb known as the slosh "danger zone" was used to predict stability slosh dynamics under closed-loop attitude control [9]. In a space vehicle with a single centerline slosh tank under thrust vector control, the "danger zone" occurs when the slosh mass location is between the vehicle center of gravity (CG) and the center of percussion, also called the instantaneous center of rotation. The center of percussion is the point along a rotating body where the combined effects of rotation and translation result in no translational motion at that point. If the slosh force application point is inside the danger zone, the slosh mass has unfavorable phasing with respect to rigid body control.

Recent advances [4] showed that the aft end of the danger zone extends beyond the center of gravity and is determined by the proper axial acceleration of the vehicle, or k_3 and $\bar{g}_0$:

$$-\frac{k_3(m_T - m_{sj})}{m_T^2 \omega_{sj}^2} < r_{sjx} < -\frac{I_T}{m_T l_g} \tag{13}$$

where the term $-\frac{I_T}{m_T l_g}$ is a center of percussion with reference to the center of gravity and l_g is length of $\vec{r}_g$, which is the location vector of the thrust vector control gimbal with respect to the vehicle center of gravity. The term $\frac{k_3(m_T - m_{sj})}{m_T^2 \omega_{sj}^2}$ is the aft limit of the danger zone, measured with reference to the center of gravity. Assuming $m_T >> m_{sj}$, it is interesting to observe that aft limit term is equal to length of pendulum

$$\frac{k_3}{\omega_{sj}^2} = L_{Pj} \tag{14}$$

This shows that using the location of the pendulum hinge point for a danger zone analysis without modifying the danger zone using the aft limit term $\frac{k_3(m_T - m_{sj})}{m_T \omega_{sj}}$ is equivalent to the danger zone for the location of the MSD slosh mass, including the modification of the aft limit. However, the upper boundary of the danger zone must be maintained the same as demonstrated by [7] where the slosh dynamic is favorably phased when the slosh mass is above the center of percussion for the pendulum case. To use slosh pendulum hinge point as the analysis point, the length of pendulum can be simply added to the upper boundary.

The updated danger zone limits for the pendulum model, using the pendulum hinge point as the reference for analysis measured with respect to the center of gravity of the vehicle, are presented below.

$$0 < r_{Pjx} < -\frac{I_T}{m_T l_g} + \frac{k_3}{\omega_{sj}^2} \tag{15}$$

Therefore, even when the points of force application for the slosh differ between the pendulum and MSD cases, the modified danger zone, determined by the location of the slosh mass as shown in Equation 13, remains consistent. This holds true regardless of the type of mechanical analogy employed in the models.

Implications to the Common Modeling Practice

Earth's launch vehicles are large and have slower dynamics; the dynamics are often simplified with assumptions for easier analysis. One must be careful when implementing different slosh me-

chanical models in the equations of motion. For example, [1] shows the derivation of the integrated formulation for the multi-actuated flexible rocket vehicle including slosh, which was intended to closely capture multibody formulation but with easier analysis and fewer constraints. The integrated equation uses the MSD slosh model where it does not include the term that directly refers to the torque effect due to the slosh mass lateral offset, instead the mass property of the integrated system includes the slosh mass such that the torque effect is captured in a different way. If the resultant MSD slosh is directly replaced with the pendulum model equation of motion, it would incorrectly double book keep the k_3 torque effect. The dynamic will otherwise be corrected if case (b) was used instead as shown in Figure 1b.

GLASS SIMULATION RESULTS

Both the MSD and pendulum math models described above, including damping effects, were integrated into a 6-DOF vehicle simulation. Slosh lateral displacement results of 500-case descent and landing Monte Carlo runs are shown in Figures 11 - 14 below.

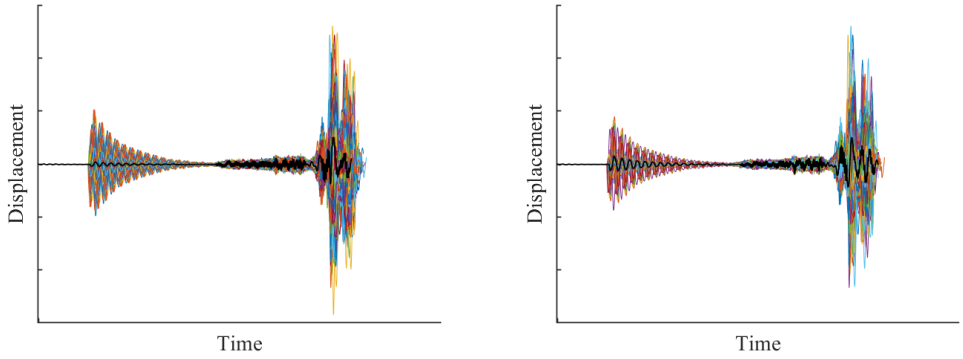

(a) MSD Model (b) Pendulum Model

Figure 11: Integrated Model Simulation Results, Tank 1, Y axis

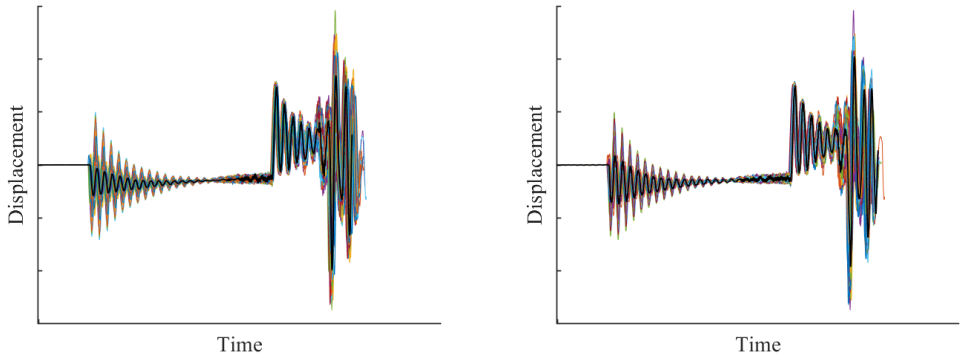

(a) MSD Model (b) Pendulum Model

Figure 12: Integrated Model Simulation Results, Tank 1, Z axis

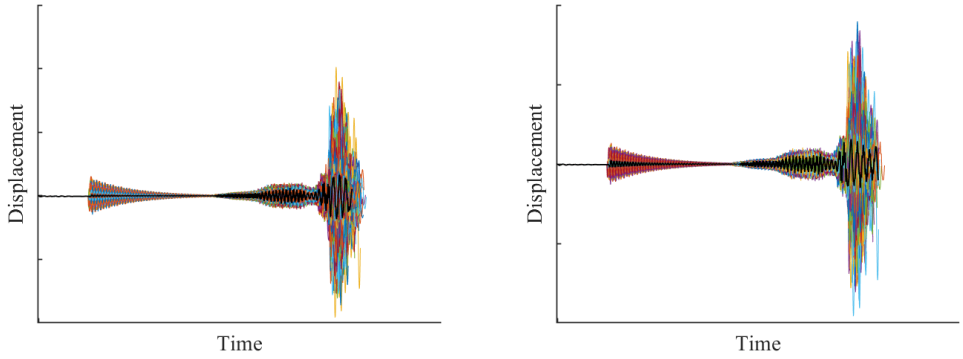

(a) MSD Model (b) Pendulum Model

Figure 13: Integrated Model Simulation Results, Tank 2, Y axis

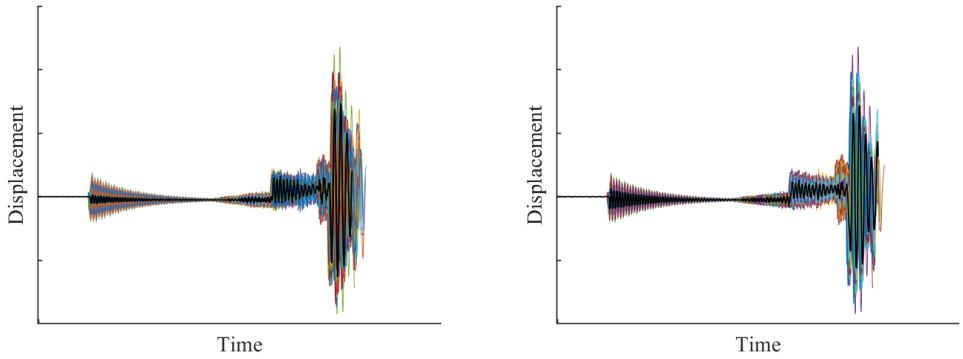

(a) MSD Model (b) Pendulum Model

Figure 14: Integrated Model Simulation Results, Tank 2, Z axis

As shown in Figures 11 - 14, the slosh dynamics in the integrated sim show similar bulk motion characteristics between the two models. This also aligns with linear stability analysis in terms of the slosh stability. The match between two mechanical models Monte Carlo results and alignment with the stability analysis brings higher confidence of both mechanical models, and the derivation and implementation of the multi-body dynamic.

CONCLUSION

The dynamics of slosh mechanical analogies in high-gravity regimes is often simplified for space vehicles, particularly large launch vehicles. This paper re-derives the equations of motion capturing non-linearity and secondary effects, to provide a more accurate representation. The equations of motion for both pendulum and MSD models were validated using MathWorks® Simscape™ Multibody™ toolbox, increasing confidence in both the derived equations and GLASS's Simscape™ Multibody™ capability. This approach ensures that slosh dynamics can be accurately demonstrated via slosh modeling through the Simscape™ Multibody™ set-up.

Furthermore, pendulum and MSD mechanical analogies were analyzed in-depth and the findings regarding these analogies for a vehicle used for ascent, descent and landing are:

1. The pendulum mass located at the same level as MSD mass captures equivalent resultant force and torque applied to the main body; therefore, it is a recommended approach for a proper multi-body dynamic.

2. When the pendulum model is used in the multi-body or integrated EOM, the torque effect due to the lateral slosh offset does not need to be taken into account in the EOM or analysis, such as the danger zone analysis.

Future works include validating derived equations of motion for multiple slosh masses with higher degree of freedom tank constraints, higher fidelity dynamic for phases involving fast maneuvers, refining pendulum damping term to match the MSD damping term or nonlinear damping effect as observed by CFD and experiments and further analysis for proper implementation of mechanical models for other configurations such as fast maneuvering trajectory and off-centerline multi-tank setting.

ACKNOWLEDGMENT

The authors would like to acknowledge Brock Cazalet for deriving alternative 6-DOF pendulum model equations of motion using the Lagrange method, Justin Ganiban for his initial work on implementing the slosh model in GLASS, Jing Pei for reviewing the MSD equations of motion, Jorge Munoz-Burgos for discussions on alternative verification methods, Mark Jackson for his supervisory support, John McCullough for providing ESSCA contractor support, and NASA Human Landing System (HLS) program for supporting this activity.

REFERENCES

[1] J. Orr, "A Flight Dynamics Model for a Multi-Actuated Flexible Rocket Vehicle," *AIAA Atmospheric Flight Mechanics Conference*, No. 2011–6563, 2011.

[2] F. T. Dodge, *The New Dynamic Behavior of Liquids in Moving Containers*. San Antonio, Texas: Southwest Research Institute, 2000.

[3] N. Aeronautics and S. Administration, *Propellant Slosh Loads*. Hampton, Virginia: National Aeronautics and Space Administration, 1968.

[4] J. A. Ottander, R. A. Hall, and J. F. Powers, "Practical Methodology for the Inclusion of Nonlinear Slosh Damping in the Stability Analysis of Liquid-propelled Space Vehicles," *AIAA SciTechForum*, No. 2018-2097, 2018.

[5] H. N. Abramson, H. F. Bauer, G. W. Brooks, W. h. Chu, and J. F. Dalzell, *The Dynamic Behavior of Liquids in Moving Containers*. Washington, D.C.: National Aeronautics and Space Administration, 1966.

[6] J. A. Frosch and D. P. Vallely, "Saturn AS-501/S-IC Flight Control System Design," *Journal of Spacecraft*, Vol. 4, No. 8, 1967, pp. 1003–1009.

[7] J. Pei, "Analytical Investigation of Propellant Slosh Stability Boundary on a Space Vehicle," *Journal of Spacecraft and Rockets*, Vol. 58, No. 5, 2021.

[8] J. Orr, "State Space Implementation of Linear Pertubation Dynamic Equations for Flexible Launch Vehicles," *AIAA Guidance, Navigation, and Control Conference*, No. 2009–5962, 1967.

[9] H. F. Bauer, "Stability Boundaries of Liquid-Propelled Space Vehicles with Sloshing," *Journal of Spacecraft*, Vol. 1, No. 7, 1967, pp. 1583–1589.

APPENDIX A

PARAMETER DEFINITIONS

$\vec{\delta}_{sj}$	MSD sloshing mass y and z-axis displacement in *j*th tank
m_{sj}	slosh mass in *j*th tank
ζ_{sj}	MSD slosh damping coefficient in *j*th tank
ω_{sj}	MSD slosh natural frequency in *j*th tank
m_T	total vehicle mass except sloshing mass
I_T	total vehicle m.o.i. except sloshing mass
$\vec{r}_{sj}$	sloshing mass location relative to the c.g.
$\vec{r}_g$	engine gimbal location to the c.g.
$\vec{\omega}$	vehicle angular velocity measured w.r.t. body axis
$\vec{v}$	vehicle linear velocity measured w.r.t. inertial axis
$\vec{a}_b$	specific acceleration measured w.r.t. body axis
$\vec{v}_{sj}$	sloshing mass linear velocity measured w.r.t. vehicle axis
$\vec{p}$	linear momentum
$\vec{h}$	angular momentum
$\vec{f}$	external force
$\vec{g}$	external moment
k_3 or $\bar{g}_0$	an axial proper acceleration term
T	thrust magnitude
β_e	pitch gimbal angle
$\vec{T}_e$	thrust vector
$\vec{r}_{Pj}$	pendulum hinge point relative to the c.g. in *j*th tank
$\vec{l}_{Pj}$	pendulum arm vector in *j*th tank
L_{Pj}	pendulum arm length in *j*th tank
θ_{Pj}	pendulum pitch angle w.r.t. body axis in *j*th tank
ψ_{Pj}	pendulum yaw angle w.r.t. body axis in *j*th tank
$\vec{r}_g$ or l_g	location of the thrust vector control gimbal w.r.t. the vehicle center of gravity

APPENDIX B

SLOSH/VEHICLE MODEL DERIVATION

MSD Slosh Model Derivation

The time rate of any vector $\vec{A}$ described in terms of components relative to reference frame having angular velocity $\vec{\omega}$ is

$$\frac{\delta \vec{A}}{\delta t}|^i = \frac{\delta \vec{A}}{\delta t}|^r + \vec{\omega} \times \vec{A} \tag{16}$$

where $\frac{\delta \vec{A}}{\delta t}|^i$ is $\vec{A}$ differentiated in reference to the inertial frame, and $\frac{\delta \vec{A}}{\delta t}|^r$ is $\vec{A}$ differentiated in reference to the rotational frame. Let $\vec{p}$ be the linear momentum of a mass body measured with respect to the reference frame having angular velocity $\vec{\omega}$ where

$$\vec{p} = m\vec{v} \tag{17}$$

The derivative of $\vec{p}$ is obtained by using Eq. 16 that yields

$$\frac{\delta\vec{p}}{\delta t}|^i = \frac{\delta\vec{p}}{\delta t}|^r + \vec{\omega} \times \vec{p} \tag{18}$$

where $\frac{\delta\vec{p}}{\delta t}$ is external force as shown below.

$$\vec{f} = \frac{\delta\vec{p}}{\delta t}|^i \tag{19}$$

Thus, the rate of linear momentum differentiated with respect to the body axis is given by:

$$\dot{\vec{p}} = -\vec{\omega} \times \vec{p} + \vec{f} \tag{20}$$

where $\dot{\vec{p}}$ is defined by $\vec{p}$ differentiated with respect to the rotating body.

The linear momentum of the slosh mass is given by:

$$\vec{p}_{sj} = m_{sj}(\vec{v} - \vec{r}_{sj} \times \vec{\omega} + \dot{\vec{\delta}}_{sj}) \tag{21}$$

The external force applied to the slosh mass is given by:

$$\vec{f}_{sj} = -m_{sj}(K\vec{\delta}_{sj} + D\dot{\vec{\delta}}_{sj}) \tag{22}$$

Plugging Eq. 21 and its derivative into Eq. 20, the equation yields:

$$m_{sj}(\dot{\vec{v}} - \dot{\vec{r}}_{sj} \times \vec{\omega} - \vec{r}_{sj} \times \dot{\vec{\omega}} + \ddot{\vec{\delta}}_{sj}) = -m_{sj}\vec{\omega} \times (\vec{v} - \vec{r}_{sj} \times \vec{\omega} + \dot{\vec{\delta}}_{sj}) - m_{sj}(K\vec{\delta}_{sj} + D\dot{\vec{\delta}}_{sj}) \tag{23}$$

The term $\dot{\vec{r}}_{sj}$ can be approximated as $\dot{\vec{\delta}}_{sj}$ since the vertical component of $\vec{r}_{sj}$ is a function of the x component of the center of gravity and the fill level, which change slowly over time and can be approximated as zero. The removal of the x component of $\vec{r}_{sj}$ leaves the lateral components in the term, which coincides with $\vec{\delta}_{sj}$. Also, the rates of slosh mass $\dot{m}_{sj}$ and total mass $\dot{m}_T$ are assumed to be negligible. See Figure 2a for the kinematic properties of $\vec{r}_{sj}$ and $\vec{\delta}_{sj}$.

Rearranging Eq. 23, simplifying the equation using $\vec{a}_b = \dot{\vec{v}} + \vec{\omega} \times \vec{v}$ and $\dot{\vec{r}}_{sj} = \dot{\vec{\delta}}_{sj}$, the equation yields:

$$\ddot{\vec{\delta}}_{sj} + D\dot{\vec{\delta}}_{sj} + K\vec{\delta}_{sj} = -\vec{a}_b + \vec{r}_{sj} \times \dot{\vec{\omega}} + \vec{\omega} \times (\vec{\omega} \times \vec{r}_{sj}) - 2\vec{\omega} \times \dot{\vec{\delta}}_{sj} \tag{24}$$

where $D = 2\zeta_{sj}\omega_{sj}$ and $K = \omega_{sj}^2$. Since the slosh mass is constrained in the x body axis, Eq. 24 is applicable to the lateral (y and z) body axes only.

Assuming that there is no aerodynamic disturbance and constrained yaw, the translation equation of motion is given by

$$m_T\vec{a}_b = \vec{T}_e + m_{sj}(K\vec{\delta}_{sj} + D\dot{\vec{\delta}}_{sj}) \tag{25}$$

Where

$$\vec{T_e} = \begin{bmatrix} 0 \\ Tcos(\beta_e) \\ Tsin(\beta_e) \end{bmatrix} \tag{26}$$

Vehicle Rotation Dynamic Derivation

Using Eq. 16, the rate of rotational momentum is given by:

$$\frac{\delta \vec{h}}{\delta t}|^i = \frac{\delta \vec{h}}{\delta t}|^r + \vec{\omega} \times \vec{h} \tag{27}$$

The external torque is given by

$$\vec{g} = \frac{\delta \vec{h}}{\delta t}|^i \tag{28}$$

The rate of change of rotational momentum differentiated with respect to the body axis is given by:

$$\dot{\vec{h}} = -\vec{\omega} \times \vec{h} + \vec{g} \tag{29}$$

where $\dot{\vec{h}}$ is defined by $\vec{h}$ differentiated with respect to the rotating body.

The rotational momentum of the vehicle is given by:

$$\vec{h} = I_T \vec{\omega} \tag{30}$$

The momentum of the vehicle is given by:

$$\vec{p} = m_T \vec{v} \tag{31}$$

The external torque applied to the vehicle from slosh dynamic is given by:

$$\vec{g} = \vec{r}_{sj} \times \vec{f_v} + \vec{r}_g \times \vec{T_e} \tag{32}$$

where $\vec{f_v}$ is force applied to vehicle by the slosh mass such that

$$\vec{f_v} = -\vec{f} \tag{33}$$

From Eqs. 22 and 23, the term $\vec{f_v}$ deduces to

$$\vec{f_v} = m_{sj}(-\ddot{\vec{\delta}}_{sj} - \vec{a}_b + \vec{r}_{sj} \times \dot{\vec{\omega}} + \vec{\omega} \times (\vec{\omega} \times \vec{r}_{sj}) - 2\vec{\omega} \times \dot{\vec{\delta}}_{sj}) \tag{34}$$

Thus, the Eq. 34 becomes

$$\vec{g} = m_{sj}\vec{r}_{sj} \times (-\ddot{\vec{\delta}}_{sj} - \vec{a}_b + \vec{r}_{sj} \times \dot{\vec{\omega}} + \vec{\omega} \times (\vec{\omega} \times \vec{r}_{sj}) - 2\vec{\omega} \times \dot{\vec{\delta}}_{sj}) + \vec{r}_g \times \vec{T}_e \tag{35}$$

Plugging Eq. 25, its derivative, Eqs. 26 and 30 into Eq. 24, the equation yields,

$$\begin{aligned} I_T\dot{\vec{\omega}} = -\vec{\omega} \times I_T\vec{\omega} - m_{sj}\vec{r}_{sj} \times \vec{a}_b - m_{sj}\vec{r}_{sj} \times \ddot{\vec{\delta}}_{sj} + m_{sj}\vec{r}_{sj} \times (\vec{r}_{sj} \times \dot{\vec{\omega}}) \\ + m_{sj}\vec{r}_{sj} \times (\vec{\omega} \times (\vec{\omega} \times \vec{r}_{sj})) - 2m_{sj}\vec{r}_{sj} \times (\vec{\omega} \times \dot{\vec{\delta}}) + \vec{r}_g \times \vec{T}_e \end{aligned} \tag{36}$$

From the previous section, the term $\dot{\vec{r}}_{sj}$ can be approximated as $\dot{\vec{\delta}}_{sj}$. Also, the rates of slosh mass ($\dot{m}_{sj}$), vehicle/tank total mass ($\dot{m}_T$) and vehicle/tank total inertia tensor ($\dot{I}_T$) are assumed to be negligible.

Pendulum Slosh Model Derivation

Because the fixed pendulum length prevents translational motion with respect to the pivot, continuing from equation 7:

$$\Sigma\vec{M} = I\dot{\vec{\omega}} + \vec{\omega} \times I\vec{\omega} \tag{37}$$

The angular quantities are a combination of the pendulum states and the vehicle states:

$$\Sigma\vec{M} = I(\dot{\vec{\omega}} + \ddot{\vec{\theta}}_{Pj}) + (\vec{\omega} + \dot{\vec{\theta}}_{Pj}) \times I(\vec{\omega} + \dot{\vec{\theta}}_{Pj}) \tag{38}$$

The torques acting on the slosh mass consist of the sources of acceleration of the pivot point. These are:

- forces acting on the vehicle—these include thrust T as well as any lateral disturbance force
- the effect of vehicle angular acceleration, $\dot{\vec{\omega}} \times \vec{r}_{Pj}$
- the effect of vehicle angular velocity, $\vec{\omega} \times (\vec{\omega} \times \vec{r}_{Pj})$

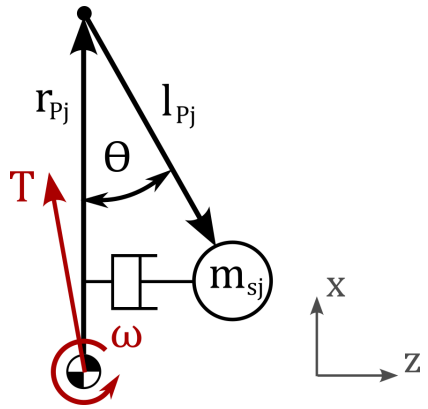

Figure 15: Sources of acceleration of the pivot point

Incorporating these moments into equation 38:

$$\vec{l}_{Pj} \times \left(\frac{\vec{T}}{m_T} - \dot{\vec{\omega}} \times \vec{r}_{Pj} - \vec{\omega} \times (\vec{\omega} \times \vec{r}_{Pj}) \right) m_{sj} = I(\dot{\vec{\omega}} + \ddot{\vec{\theta}}_{Pj}) + (\vec{\omega} + \dot{\vec{\theta}}_{Pj}) \times I(\vec{\omega} + \dot{\vec{\theta}}_{Pj}) \quad (39)$$

Note that the coriolis acceleration term $2\vec{\omega} \times \vec{v}_{sj}$ (not shown) would be along the pendulum vector; this is because the velocity of the slosh mass can only be in the tangential direction. As such, the coriolis acceleration cannot produce a torque about the pivot and can be neglected.

Since slosh is modeled as a point mass, the slosh inertia with respect to the pivot point is given by:

$$I = \begin{bmatrix} |\vec{l}_{Pj}|_{yz}{}^2 m_{sj} & 0 & 0 \\ 0 & |\vec{l}_{Pj}|_{xz}{}^2 m_{sj} & 0 \\ 0 & 0 & |\vec{l}_{Pj}|_{xy}{}^2 m_{sj} \end{bmatrix} \quad (40)$$

Because the I matrix is diagonal, the $(\vec{\omega} + \dot{\vec{\theta}}_{Pj}) \times I(\vec{\omega} + \dot{\vec{\theta}}_{Pj})$ term is a cross-product of parallel vectors, which is zero. Simplifying and solving for $\ddot{\vec{\theta}}_{Pj}$:

$$\ddot{\vec{\theta}}_{Pj} = \frac{\vec{l}_{Pj} \times \left(\frac{\vec{T}}{m_T} - \dot{\vec{\omega}} \times \vec{r}_{Pj} - \vec{\omega} \times (\vec{\omega} \times \vec{r}_{Pj}) \right)}{|\vec{l}_{Pj}|^2} - \dot{\vec{\omega}} \quad (41)$$

The motion of the slosh mass affects vehicle motion via force transmitted through the pendulum to the pivot point, given by:

$$\vec{f} = m_{sj}\left(-\vec{a}_s - \dot{\vec{\omega}}|_{sj}\right) \tag{42}$$

Where $\vec{a}_s$ is the acceleration of the slosh mass in the vehicle frame:

$$\vec{a}_s = \ddot{\vec{\theta}}_{Pj} \times \vec{l}_{Pj} + \dot{\vec{\theta}}_{Pj} \times \dot{\vec{\theta}}_{Pj} \times \vec{l}_{Pj} + 2\vec{\omega} \times \left(\dot{\vec{\theta}} \times \vec{l}_{Pj}\right) \tag{43}$$

And $\dot{\vec{\omega}}|_s$ is the total acceleration of the vehicle (including rotation) at the slosh location, expressed in the vehicle frame:

$$\dot{\vec{\omega}}|_s = \vec{a}_b + \dot{\vec{\omega}} \times \left(\vec{r}_{Pj} + \vec{l}_{Pj}\right) + \vec{\omega} \times \left[\vec{\omega} \times \left(\vec{r}_{Pj} + \vec{l}_{Pj}\right)\right] \tag{44}$$

Where $\vec{a}_b$ is the vehicle acceleration at the center of gravity. Incorporating equations 43 and 44 into equation 42 yields a formulation of the force to apply to the vehicle at the pivot point:

$$\begin{aligned}\vec{f} = m_{sj}\Big\{&-\ddot{\vec{\theta}}_{Pj} \times \vec{l}_{Pj} - \dot{\vec{\theta}}_{Pj} \times \dot{\vec{\theta}}_{Pj} \times \vec{l}_{Pj} - 2\vec{\omega} \times \left(\dot{\vec{\theta}} \times \vec{l}_{Pj}\right) \\ &-\vec{a}_b - \dot{\vec{\omega}} \times \left(\vec{r}_{Pj} + \vec{l}_{Pj}\right) - \vec{\omega} \times \left[\vec{\omega} \times \left(\vec{r}_{Pj} + \vec{l}_{Pj}\right)\right]\Big\}\end{aligned} \tag{45}$$

Pendulum Damping Coefficient

To the authors' knowledge, there is no existing literature that specifically derives a pendulum damping coefficient that translates to the damping effect observed in a MSD damping system. To achieve pendulum damping that closely approximates MSD damping, the lateral component of the pendulum's mass velocity is considered. The lateral damping force (f_{sjd}) and the resultant pendulum damping torque (g_{sjd}) are expressed as:

$$f_{sjd} = 2m_{sj}\zeta\omega_n\dot{\delta} = 2m_{sj}\zeta\omega_n\dot{\theta}_{Pj}L_{Pj}cos(\theta_{Pj}) \tag{46}$$

$$g_{sjd} = \vec{l}_{Pj} \times f_{sjd} = 2m_{sj}\zeta\omega_n\dot{\theta}_{Pj}L_{Pj}^2cos^2(\theta_{Pj}) \tag{47}$$

To incorporate the effects of damping into the pendulum dynamics, the Equation 47 will be added to the lateral disturbance force F_d shown in Equation 41